SUPPRESSING ELECTRON MULTIPACTING IN COAXIAL LINES BY DC VOLTAGE

Pasi Ylä-Oijala
Rolf Nevanlinna Institute
University of Helsinki, Finland

November 5, 1997

Abstract

In this report the effect of DC biasing voltage to electron multipacting in coaxial lines is studied numerically. Both the standing waves and traveling waves as well as a combination of the standing and traveling waves are considered. We show that it is possible to suppress multipacting in coaxial lines by an appropriately chosen biasing voltage. We give simple scaling laws for the biasing voltage with respect to the outer diameter, impedance and frequency of the line. These scaling laws together with our previously found scaling laws for the MP power levels can be used to determine an optimal suppressing DC voltage for any coaxial line with any wave form. Furthermore, certain DC voltages are found to generate a new type of one-point multipacting on the inner conductor of the line. The numerical calculations of this report were carried out during the joint project of Rolf Nevanlinna Institute and Deutsches Electronen-Synchrotron (DESY).

1 Introduction

Electron multipacting (MP) can cause loss of the field power and it can break the high power rf components like couplers and windows. This phenomenon starts if certain resonant conditions for electron trajectories are fulfilled and if the impacted surface has a secondary yield larger than one. A general cure against MP is to avoid the resonant conditions by an appropriate design of the geometry. Further, there are certain coating techniques to reduce the secondary yield to lower levels. The resonance conditions for MP are

(1) An electron emitted from the cavity wall is driven by the EM fields and returns back after an integer number of rf cycles to the same point of the cavity wall.
(2) The impacting electron produces more than one secondary electron.

In the previous reports [1] on standing waves (SW) and [4] on traveling (TW, and mixed waves (MW), we investigated the dynamics of the electron trajectories in order to recognize those rf power levels when MP may occur in the given geometry. For straight coaxial lines, we found simple scaling laws for the MP power bands with respect to the diameter, frequency and impedance of the line. By these laws, one can shift the MP bands by altering the design of the line in an appropriate way.

In many cases, however, it is not possible to change the design of the line. Therefore, it is important to know the effect of different suppressing methods to MP by perturbating the rf fields. The idea is to perturb the rf field either by modifying the geometry or the field itself to break the MP conditions. This usually leads to breaking the stable trajectories or forcing the impact energies to low secondary yield bands.

In this report, we analyze the effect of DC biasing voltage to MP in coaxial lines. The DC biasing voltage is a static electric perturbation which generates a repelling radial force. We show that with our MP analysis method, it is possible to optimize the biasing voltage to achieve acceptably low multipacting levels. Both the SW and TW operations as well as a combination of the SW and TW operations are considered. We also give simple scaling laws for the biasing voltage with respect to the diameter, frequency and impedance of the line. By these laws, one can choose an optimal biasing voltage to suppress multipacting in any coaxial line. In the numerical computations we have considered the 1.3 GHz, 50 Ω coaxial line with the outer diameter of 40 mm, if not mentioned otherwise. The main results of the research will be presented also in the forthcoming paper [3]. For the used numerical methods we refer to [1] and [3]. The secondary yield function used through out this report is a typical curve for the niobium surface, [1].

2 Multipacting in coaxial lines

Our previous analysis in [1] shows that in the SW multipacting appears always close to the maximum of the electric field. This kind of MP, which is predominantly due to the electric field only, is called the *electric multipacting* (EMP). Further, we recognized two different dominant types of MP. First, there are one–point MP processes of different order on the outer conductor of the line. Secondly, there are two–point processes from the outer conductor to the inner one and back. We found the following scaling laws for the MP power levels

$$P_{\text{one-point}} \sim (f\,d)^4\,Z, \quad P_{\text{two-point}} \sim (f\,d)^4\,Z^2, \tag{3}$$

where f is the frequency, d is the outer diameter and Z is the impedance of the line. Thus, by increasing the impedance, for example, the multipacting power levels can be shifted upwards. These scaling laws turned out to be valid in the TW and MW operations, too.

Furthermore, in [4] we analyzed MP in the TW and MW operations. When the wave is a purely one–way traveling wave, the structure of MP power levels resembles the SW case. Similar MP processes can be recognized in both the SW and TW cases. A closer analysis of electron trajectories show that the TW MP power bands of different order appear at four times higher power values than the corresponding SW MP bands. Furthermore, in the TW operation the wall impacts of the MP electrons appear again close to the maximum of the electric field and, what is essential, the electrons are slowly traveling along with the wave as the wave form moves. Due to this traveling in the TW operation MP may occur on the entire line and MP is of mixed nature, i.e., MP is due to both the electric and magnetic fields.

When the wave is neither a purely one–way traveling wave (TW) nor perfectly reflected (SW), the MP structure is more complicated. In that case we are able to recognize two families of MP of different nature. One appears close to the maximum of the SW electric field can be identified as EMP; another appears close to the maximum of the SW magnetic field and is called the (coaxial) *magnetic multipacting* (MMP). Further, in the MW operation MP is

found to be related to certain fixed points in the phase space. In the case of EMP the fixed point is repelling in the spatial direction but attractive in the phase directions, whereas the MMP is attractive in both directions. Thus, the EMP processes are more sensitive to the perturbations of the field than the corresponding MMP processes. This might suggest that a higher DC voltage is needed to suppress MMP than the corresponding EMP. Our analysis shows, however, that this is not the case.

Furthermore, the MP electron trajectories in all cases are predominantly radial. In other words, the movement of the MP electrons in the axial direction is much smaller than in the radial direction, even when the wave is a pure TW.

3 Analysis of DC voltage

The time–harmonic rf field with time factor $e^{-i\omega t}$ is perturbed with a DC biasing voltage between the conductors so that

$$\vec{E}(x,\varphi) = \vec{E}_R(x,\varphi) + \frac{V}{r\log(b/a)}\,\vec{e}_r, \tag{4}$$

where V is the biasing voltage between the coaxial conductors, $\varphi = \omega t$ is the phase of the field, a and b are the inner and outer radii of the line and $\vec{E}_R$ is the coaxial rf electric field depending on the reflection coefficient R as follows

$$\vec{E}_R = R\vec{E}_{SW} + (1-R)\vec{E}_{TW}, \quad 0 \le R \le 1, \tag{5}$$

where

$$\begin{aligned}
\vec{E}_{SW}(x,\varphi) &= \frac{U}{2r\log(b/a)}(\cos(kz-\varphi) - \cos(kz+\varphi))\,\vec{e}_r, \\
\vec{E}_{TW}(x,\varphi) &= \frac{U}{2r\log(b/a)}(\cos(kz-\varphi))\,\vec{e}_r.
\end{aligned}$$

Here U is the voltage drop between the inner and outer conductor, $k = \omega/c = 2\pi/\lambda$ and (r,θ,z) is the representation of the field point x in cylindrical coordinates. Since the static perturbation generated by a DC voltage is purely radial, the DC voltage does not perturb the MP electrons off the stable trajectories around the fixed point, but it generates a repelling radial force, which, when properly chosen, breaks the resonant MP conditions. In the following we analyze electron MP in coaxial lines using methods derived in [1], where the rf field is perturbed by a DC biasing voltage.

3.1 Standing waves

Consider first the SW operation, i.e., $R = 1$. Here the MP analysis is restricted to the maximum of the electric field only. We fix the field power and the biasing voltage and launch a sufficiently large number of electrons in different field phases and count the number of secondary electrons able to produce new secondary electrons. This number of secondary electrons is called the *enhanced electron counter function*. The number of emitted secondary electrons depends on the impact energy and the material characteristics of the impacted surface. For more details we refer to [3] and [1].

To find the possible MP power levels we compute the enhanced electron counter with several fixed DC voltages V. Figure 1 shows the gray scale plot of the base 10 logarithm of the relative enhanced electron counter function, after 30 impacts, as a function of the incident power and biasing voltage. The voltage, given in the horizontal axis, varies from -3000 V to 2500 V. At the vertical axis is the rf incident power in kW. Note that when multipacting occurs, the logarithm of the relative enhanced function is positive, i.e., the number of the electrons is increased. This zero–line or MP–line is indicated in the plot. Furthermore, the orders of the most prominent processes are indicated in the picture.

The plot suggests that by coupling the DC biasing voltage to the incident rf power one can ramp the rf field from zero to the desired value without any MP. The scheme should be such that the ramping path in Figure 1 does not cross any of the MP bands. There are several ways to chose such a path. One simple possibility is e.g. to use a fixed biasing voltage of -2100 V. Then the first order one–point process starts around 150 kW, but the impact energy is too high and thus, the secondary yield is too low to cause MP. Another promising possibility is to use high positive voltages, higher than 2000 V. Then a process corresponding to a MP process appears above 900 kW.

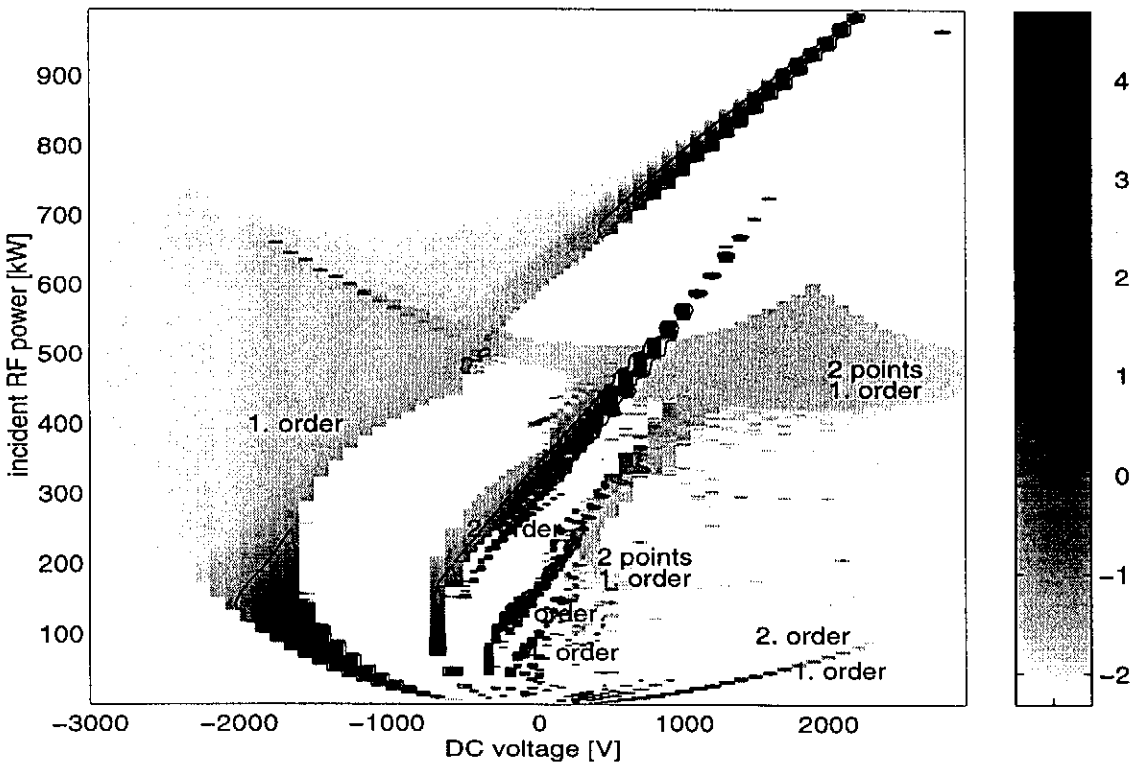

Figure 1. The gray scale plot of the 10 base logarithm of the relative enhanced counter function, after 30 impacts, as a function of the incident power (vertical axis) in kW and biasing voltage (horizontal axis) in V.

Figure 2 shows how high the rf power can be ramped with a fixed DC until the first MP process wakes up. This MP process is always a one–point process of order one and it takes place either on the outer conductor (negative voltages) or on the inner conductor (positive voltages). Close to the origin, i.e., when the voltage and rf power are both zero, the MP phenomenon is rather irregular and the curve of Figure 2 is not accurate. Figure 2 consists of

two parabolic curves. Fitting two parabolas separately to the positive and negative sides of the curve of Figure 2, in the sense of least–squares, we have found the following approximative relation between the rf power P [kW] and the biasing voltage V [V]

$$P_- \sim \left(\frac{V}{175}\right)^2 \quad \text{and} \quad P_+ \sim \left(\frac{V}{250}\right)^2 . \tag{6}$$

Here the first relation is for the negative voltages and the latter one is for the positive voltages. Note that in Figure 2 the secondary yield is ignored.

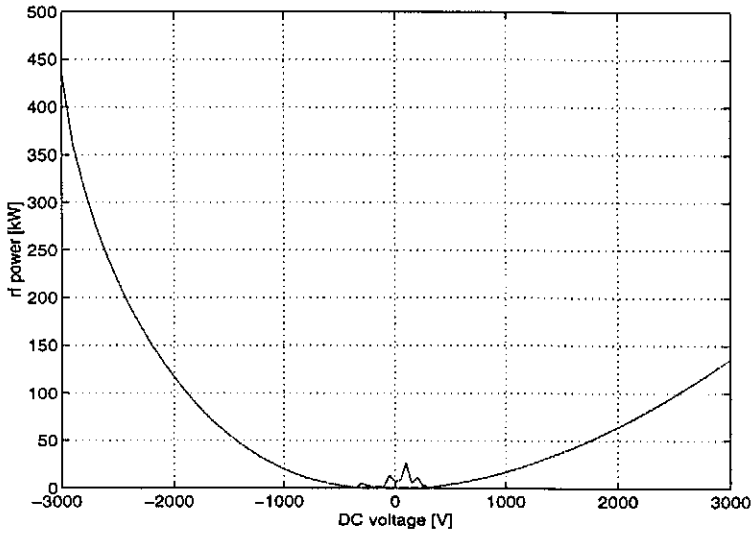

Figure 2. The curve shows the highest rf power level which can be reached without crossing any of the MP bands of Figure 1 with a fixed DC voltage.

Figure 1 shows also an other interesting feature. There exists two families of one–point processes, the one on the positive voltages (narrow bands close to the right branch of the curve in Figure 2), and the other on the negative voltages (broad bands). The latter family coincides with the processes of corresponding order of the pure SW multipacting, i.e., when $V = 0$, and the processes continue to positive voltages, too. A closer analysis of electron trajectories show the different behavior of these processes. The family on the positive side appears on the inner conductor and the family on the negative side appears on the outer conductor. Figure 3 displays the trajectories, without the biasing voltage and with the DC voltage of -1500 V and +1500 V, when the incident power is properly chosen to correspond to the one–point MP process of order one. Since, our previous computations in [1] and [4] showed that an one–point MP occurs always on the outer conductor, certain DC voltage can generate a totally new type of one–point MP on the inner conductor of the line. Note that the curvature of the trajectory increases when the rf power increases.

In [1] we have shown that without a DC voltage the MP processes appear in the reverse order when increasing the rf power, i.e., first the process of the highest order and last the first order process. However, when the DC voltage is added the situation changes. When ramping up the rf power from zero with a non–zero biasing voltage, one hits first the first order process, then the second order process, etc. This holds for both families of MP. Thus, DC voltage generates first order MP on the low rf power levels, too. This is important to know, since the first order process is the stablest one and the corresponding MP power band is the broadest

and, therefore, the first order process can cause the highest lost of the field power and other damages. However, the impact energy due to the first order process is usually rather high, especially when the voltage or the incident power is high, and the corresponding secondary yield might be rather low. This phenomenon is clearly seen in Figure 1, since there are wide bands corresponding to the first order processes, but the secondary yield is in many cases too high to cause MP. Thus, the impact energy plays again a crucial role in the process. Note that, in this geometry, the two–point processes are not MP. Figure 1 shows also that the higher order processes appear predominantly close to the zero voltage. In particular, in the negative voltage region, only the first order processes appear, when (the absolute value of) the voltage is higher that -1000 V.

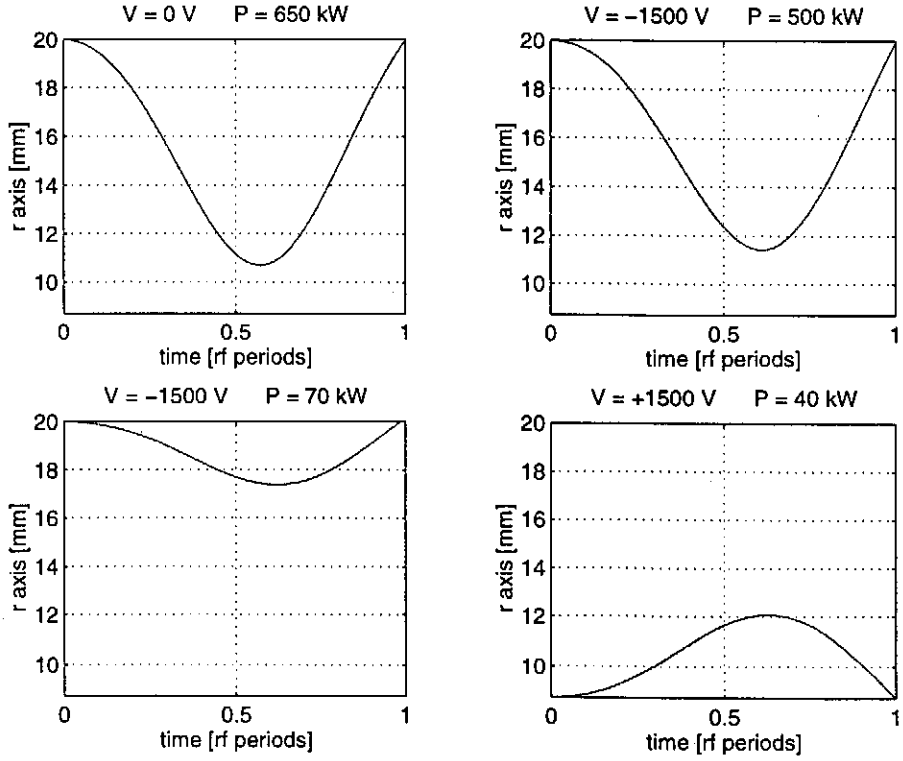

Figure 3. Electron trajectories in radius / time scale due to the one–point process of order one. The first picture on the top–left shows the trajectory without the DC bias. The pictures on the top–right and bottom–left give the trajectories when DC voltage is -1500 V and the rf power is 500 kW (top) and 70 kW (bottom). Finally the last picture shows the trajectory when the DC voltage is +1500 V and the rf power is 40 kW. In all pictures the upper and lower borders of the pictures correspond to the outer and inner conductors of the line and the electrons are initiated from the maximum of the electric field.

3.2 Traveling and mixed waves

Next the DC biasing voltage is applied to suppress MP in the TW ($R = 0$) and MW ($0 < R < 1$) operations. Figure 4 shows the base 10 logarithm of the relative enhanced electron counter in the TW operation as a function of the rf incident power and the DC biasing voltage. The figure is surprisingly identical with the SW case, Figure 1. The distribution of MP bands

remains the same, but the rf power scales by factor four. This agrees with our previously found scaling law [2]

$$P_{TW} = 4P_{SW}. \tag{7}$$

Note that the DC voltage does not depend on the reflection coefficient.

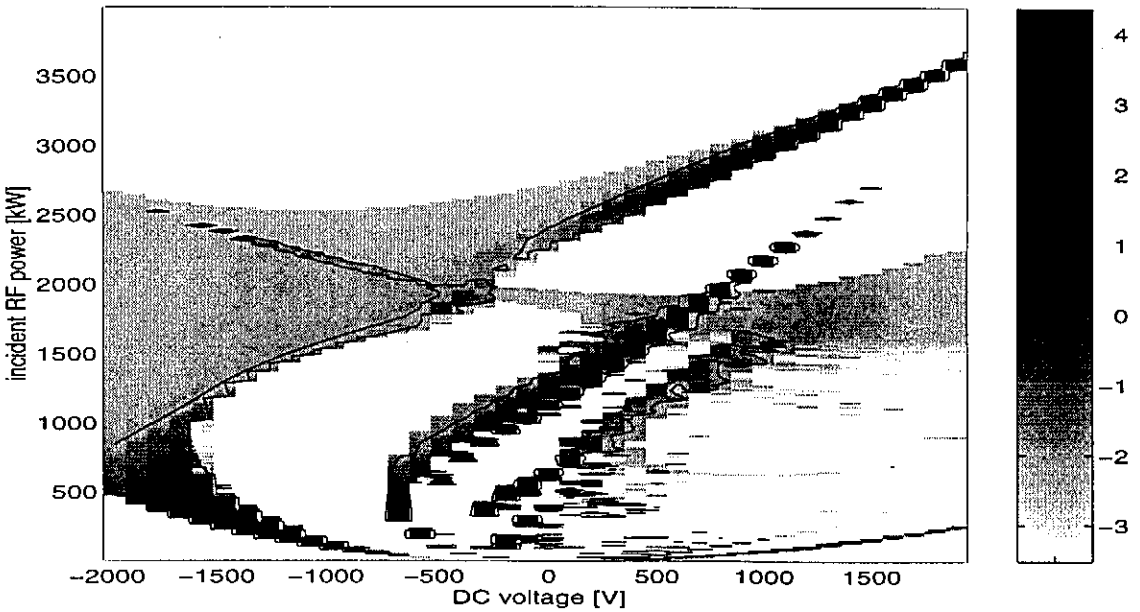

Figure 4. The gray scale plot of the base 10 logarithm of the relative enhanced counter function, after 30 impacts, as a function of the incident power (vertical axis) in kW and biasing voltage (horizontal axis) in V. The computations correspond to the 500 MHz, 50 Ω coaxial line with the outer diameter of 103 mm, in the TW operation, i,e., $R = 0$.

Figures 5 - 7[1] show the base 10 logarithm of the relative enhanced electron counters when the wave is partially reflected, corresponding to the reflection coefficients $R = 0.25$, 0.5 and 0.75. One can still find similar MP structure as in the SW and TW cases. This structure corresponds to the EMP processes of different type and order. There are also other bands which correspond to the MMP processes of different type and order. These other bands are shifting very rapidly to very high power levels when R increases. Furthermore, the EMP and MMP processes are merged together in the TW operations, as it happens without a biasing voltage. The EMP structure scales according to our previously found scaling law [3] ([4])

$$P_R^{EMP} \sim \frac{1}{(1+R)^2} P_{TW} = \frac{4}{(1+R)^2} P_{SW}. \tag{8}$$

To summarize the situation we note that a fixed biasing voltage -2100 V seems to suppress MP in all combinations of the SW and TW operations. Although an one-point MP process of order one starts at a certain power value, the power depending on the reflection coefficient R according to the rule (8), the secondary yield is always less than one and the process is not MP. In particular, the SW MP pattern of Figure 1 gives an universal lower limit for MP

[1] Computations in Figures 4 - 7 correspond to the 500 MHz, 50 Ω, 103 mm coaxial line, which according to our scaling laws gives the same MP levels as the 1.3 GHz, 50 Ω, 40 mm line.

with all possible wave forms. In other words, when the wave is switched from SW to TW, the MP power bands of Figure 1 scales upwards according to the rule (8) and the biasing voltage suggested by Figure 1 (or 2) suppress MP in all kind of wave forms.

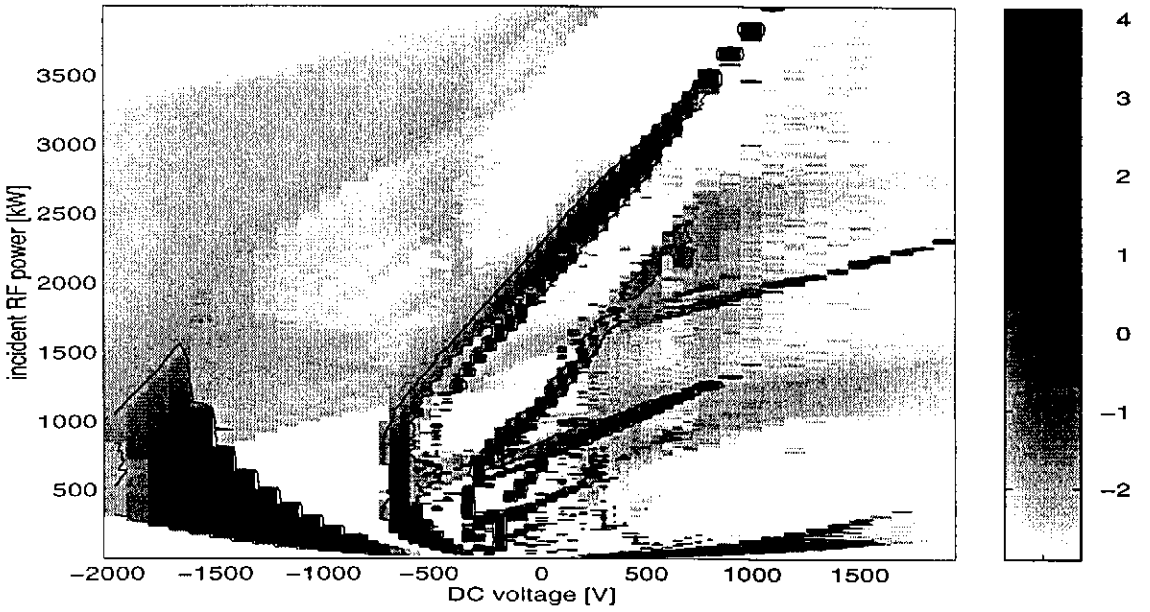

Figure 5. The gray scale plot of the base 10 logarithm of the relative enhanced counter function, after 30 impacts. The computations correspond to the 500 MHz, 50 Ω, 103 mm coaxial line, when the reflection coefficient is 0.25.

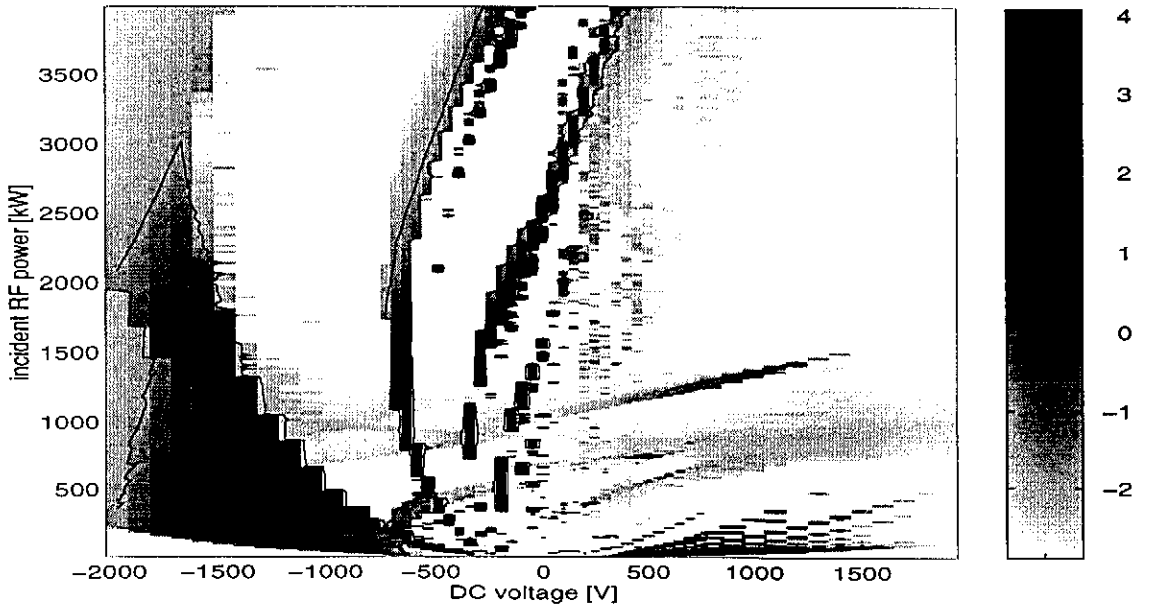

Figure 6. The gray scale plot of the base 10 logarithm of the relative enhanced counter function, after 30 impacts. The computations correspond to the 500 MHz, 50 Ω, 103 mm coaxial line, when the reflection coefficient is 0.5.

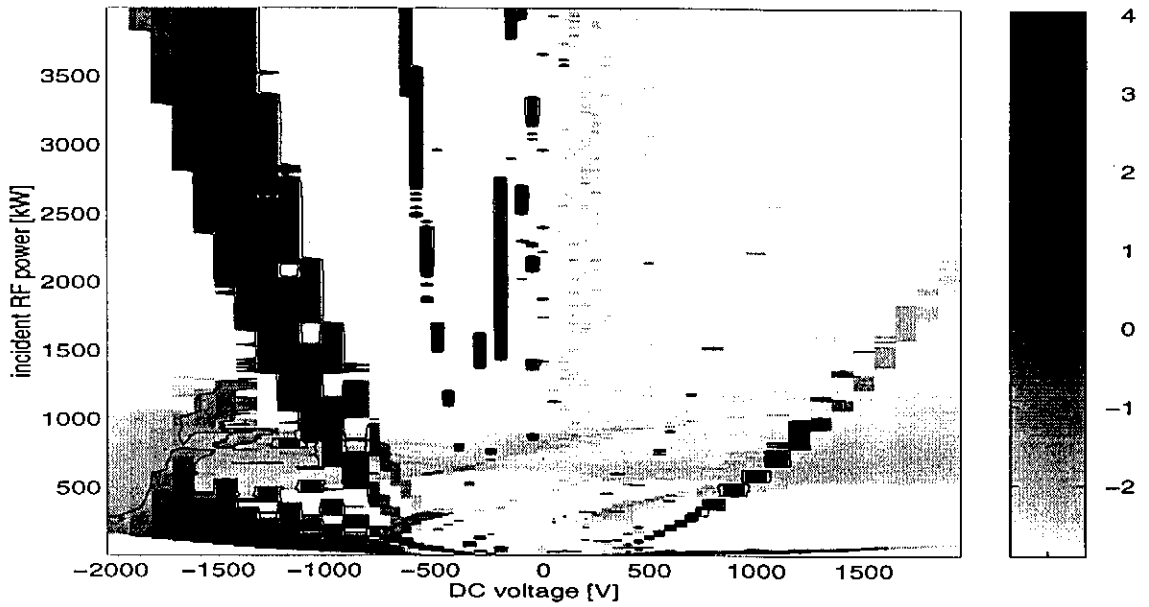

Figure 7. The gray scale plot of the base 10 logarithm of the relative enhanced counter function, after 30 impacts. The computations correspond to the 500 MHz, 50 Ω, 103 mm coaxial line, when the reflection coefficient is 0.75.

3.3 Scaling laws

In this section we study how the MP power bands of Figure 1 change when the dimensions and frequency of the line are varied. We give the scaling laws for the DC voltage with respect to the frequency of the field, impedance and diameter of the line. In this section, the computations are restricted to the maximum of the electric field in the SW operation.

First the repeat the calculation of Figure 1 with a different diameter. Figure 8 shows the gray scale plot of the base 10 logarithm of the relative enhanced electron counter function, after 30 impacts, for the 62 mm line ($Z = 50\,\Omega$ and $f = 1.3$ GHz). Figure 8 shows clearly, when compared with Figure 1, that the MP structure remains the same but the incident power scales like d^4 and the DC voltage scales like d^2. Then, we repeat the calculations of Figure 1 with the 70 Ω line and thereafter, with the frequency of 1.6 GHz, see Figures 9 and 10, respectively. Again the MP structure remains basically the same, but the incident power scales like $f^4\,Z$ (one–point processes) or $f^4\,Z^2$ (two–point processes) and the DC voltage scales like $f^2\,Z$ or $f^2\,Z^2$.

Next we more systemically analyze the effect of varying the dimensions of the line and the frequency of the field. We do not repeat the calculations of Figure 1 with all possible parameters, but with a fixed rf power. We fix the diameter, impedance and frequency as 40 mm, 50 Ω and 1.3 GHz, respectively, and choose the incident power $P = 400$ kW. Then, with the fixed impedance and frequency, we alter the outer diameter of the line. While altering the diameter, we also scale the incident power according to the rules (3). Then for each (d, f, Z, P) combination we calculate the MP levels by letting the biasing voltage vary. The picture on the left hand side of Figure 11 shows how the MP bands shift as the diameter and the corresponding incident power alter. Solid lines correspond to the one–point processes of order one and two, first order process on the negative voltages, and dashed lines correspond to the

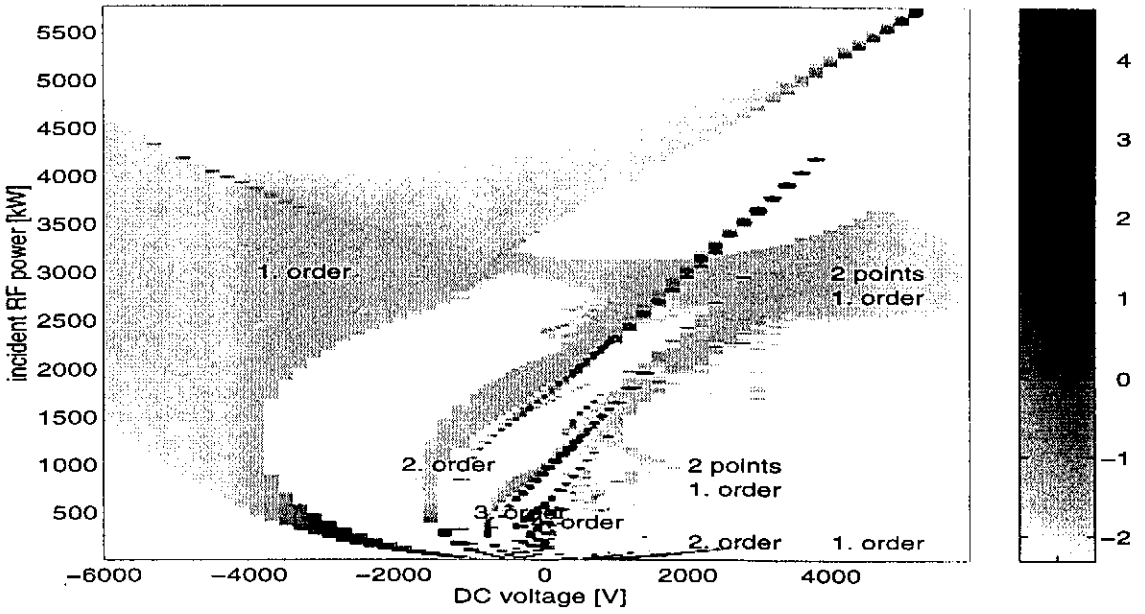

Figure 8. The gray scale plot of the base 10 logarithm of the relative enhanced counter function, after 30 impacts. The computations correspond to the 1.3 GHz, 50 Ω coaxial line with the outer diameter of 62 mm, in the SW operation.

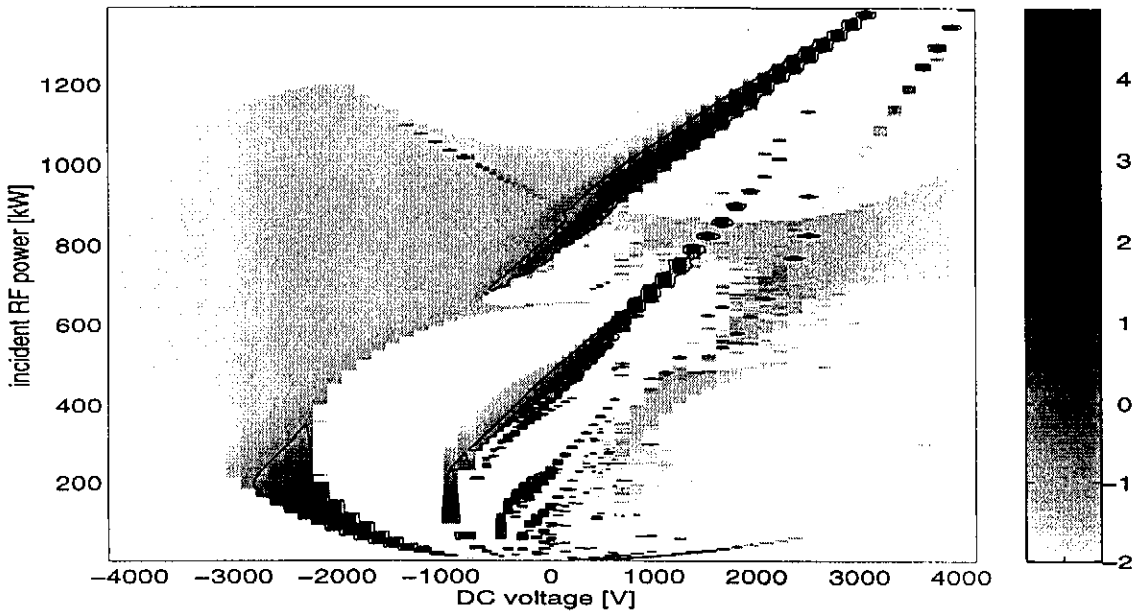

Figure 9. The gray scale plot of the base 10 logarithm of the relative enhanced counter function, after 30 impacts. The computations correspond to the 1.3 GHz, 70 Ω coaxial line with the outer diameter of 40 mm, in the SW operation.

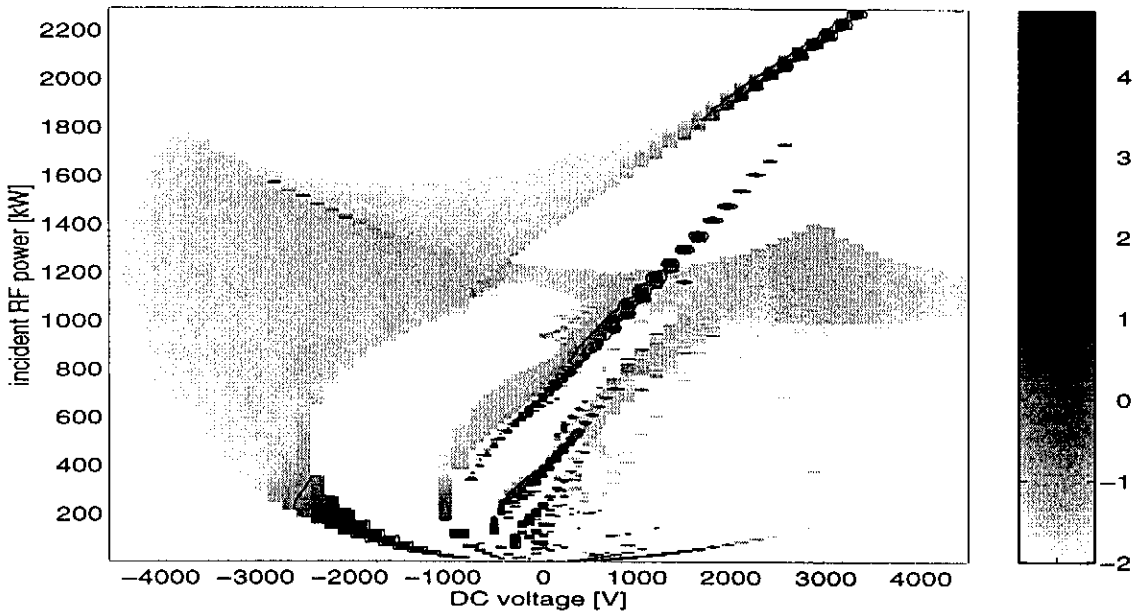

Figure 10. The gray scale plot of the base 10 logarithm of the relative enhanced counter function, after 30 impacts. The computations correspond to the 1.6 GHz, 50 Ω coaxial line with the outer diameter of 40 mm, in the SW operation.

two–point process of order one. MP occurs between the plotted lines. The figure suggests that the MP bands depend quadratically on the outer diameter. Thereafter, we alter the frequency and impedance, respectively. The picture on the right hand side of Figure 11 shows how the MP bands behave when the frequency varies. Similarly Figure 12 shows the behavior of the MP bands as the line impedance varies. Figures 11 and 12 suggest that the MP voltage bands depend quadratically on the frequency and linearly on the line impedance for the one point processes and quadratically for the two point processes.

The conclusion is that the multipacting bands shown in Figure 1 remain the same but they scale according to the following rules. The y axis of the figure, i.e., the incident rf power obeys the previously found scaling laws (3) and the x axis of the figure, i.e., the biasing voltage scales like

$$V_{\text{one-point}} \sim (f\,d)^2\,Z, \quad V_{\text{two-point}} \sim (f\,d)^2\,Z^2, \tag{9}$$

where f is the frequency, d is the outer diameter, Z is the impedance of the line and V is the biasing voltage. Thus, the above scaling laws together with the scaling laws for the incident power (3), can be used to determine multipacting bands of Figure 1 for any coaxial line with the SW operation. Furthermore, when the wave switches from the SW to the TW, and vice versa, the dependence of the multipacting bands of Figure 1 on the reflection coefficient can be descried by our previously found formula (8). Of course, when the wave is partially reflected this gives an incomplete picture, since there are also processes which are of magnetic nature. The MMP power / voltage levels shift again very rapidly to very high power regions and, especially, a magnetic process appears always on a higher power level than the corresponding electric process.

The scaling laws show also, that by increasing the impedance or outer diameter of the line, for example, the MP power levels can be shifted upwards. But, on the other hand, the DC

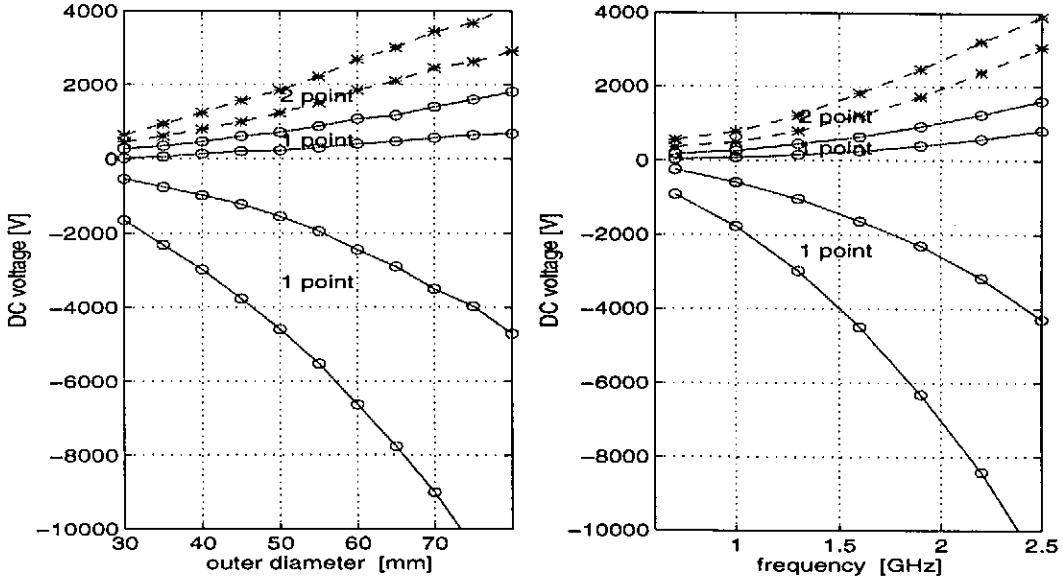

Figure 11. On the left, the curves indicate the effect of varying the diameter of the line to the MP bands. Solid lines correspond to the one–point processes of order one and two, and the dashed lines correspond to the two–point process of order one. MP occurs between the lines. On the right, the curves indicate the effect of varying the frequency of the field, respectively.

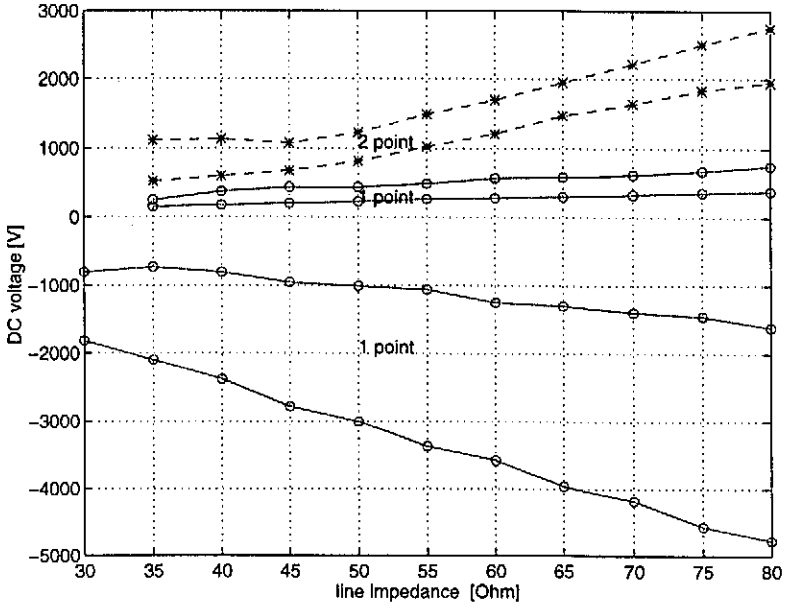

Figure 12. The bounds of each MP band with different line impedances. Note that on the low impedances, the situation starts to resemble two parallel electrodes and the MP processes do not behave regularly.

voltage which is needed to suppress MP in that new design increases, too.

The impact energy of MP electrons as well as the secondary yield depends on the dimensions of the line, frequency of the field and the biasing voltage, too. From Figures 1 and 8 one can read, for example, that MP is suppressed when the voltage is -2100 V for the 40 mm line (Figure 1) and -3500 V for the 62 mm line, respectively. We call this voltage as a *suppressing voltage* and denote it by V_0. These computations show that the suppressing DC voltage depends roughly linearly on the diameter of the line. The results of Figures 1, 8, 9 and 10, can be summarized to the following scaling law for the suppressing DC voltage

$$V_0 \sim f\, d\, Z. \tag{10}$$

Thus, the suppressing DC voltage depends linearly on the frequency, outer diameter and impedance of the line. In order to get a complete picture of the behavior of the secondary yield with a DC voltage, however, more computational analysis is needed.

4 Other coaxial structures

Our preliminary experiments with other coaxial structures, like ceramic windows, show that the DC voltage method is a possible choice to suppress MP in more complicated geometries, too. But, on the other hand, an improper DC voltage might generate new MP as shown in the previous sections. For Deutschesexample, in the conical FNAL window design MP is typically two point MP between the window and the outer (or inner) conductor. When the DC voltage is switched on, MP due to the window disappears, but a new MP, which is due to the DC voltage, appears if the voltage is not properly chosen.

The optimal voltage, however, depends on the dimensions of the line. The question is, what should be the optimal voltage, when the dimensions of the line varies, i.e., the cross section of the line is not homogeneous? In the case of a conical window, for example, the optimal voltage should vary on the window region, since the distance between the conductor and the window as well as the curvature of the MP electrons varies. We have not yet made any systematic analysis of the effect of DC voltage to MP in inhomogeneous geometries, but a rather safe choose might be to use a voltage which is needed to suppress MP in the straight coaxial line corresponding to the largest dimensions of the inhomogeneous line. Namely, if the voltage is high enough, it will anyhow suppress MP.

5 Summary

In this report the DC biasing voltage is numerically analyzed in coaxial lines. Both the SW and TW as well as mixed waves are considered. The DC biasing voltage turns out be an effective and simple method to suppress MP in coaxial lines. We give simple scaling laws to the biasing voltage with respect to the frequency of the field, impedance of the line and diameter of the line. By these scaling laws one can optimize the biasing DC voltage to suppress MP in any coaxial line with any wave form. Furthermore, the present analysis shows a new one–point MP on the inner conductor of the line.

However, when changing the design of the line, the MP power bands may be shifted to other power levels, but, at the same time the DC voltage needed to suppress MP changes, too. The

MP rf power and DC voltage bands depend differently on the variations of the dimensions and frequency of the line. Thus, in the case of more general structures the same DC voltage which is needed to suppress MP in one part of the coupler, can generate MP on the other part of the coupler.

Acknowledgments

The computations presented in this report were carried out in the joint project of Rolf Nevanlinna Institute, University of Helsinki, Finland and Elektronen–Synchrotron DESY, Hamburg, Germany. The author wish to thank Dr. Dieter Proch for a very good and fruitful co–operation. Also Prof. Jukka Sarvas and MSc Hannu Mäkiö are highly acknowledged for numerous enlightening discussions. I also thank Prof. Erkki Somersalo for his useful comments and suggestions during the work.

References

[1] E. Somersalo, P. Ylä–Oijala and D. Proch: Electron Multipacting in RF Structures. TESLA Reports 14–94.

[2] E. Somersalo, P. Ylä–Oijala and D. Proch: Analysis of Multipacting in Coaxial Lines. IEEE Proceedings, PAC 95, pp. 1500–1502.

[3] E. Somersalo, P. Ylä–Oijala, D. Proch and J. Sarvas: Computational Methods for Analyzing Electron Multipacting in RF Structures. To be submitted to *Particle Accelerators.*

[4] P. Ylä–Oijala: Analysis of Electron Multipacting in Coaxial Lines with Traveling and Mixed Waves. TESLA Reports (to be submitted).